

Multi-mass schemes for collisionless N -body simulations

Mimi Zhang ^{*} and John Magorrian [†]

Rudolf Peierls Centre for Theoretical Physics, 1 Keble Road, Oxford OX1 3NP

ABSTRACT

We present a general scheme for constructing Monte Carlo realizations of equilibrium, collisionless galaxy models with known distribution function (DF) f_0 . Our method uses importance sampling to find the sampling DF f_s that minimizes the mean-square formal errors in a given set of projections of the DF f_0 . The result is a multi-mass N -body realization of the galaxy model in which “interesting” regions of phase-space are densely populated by lots of low-mass particles, increasing the effective N there, and less interesting regions by fewer, higher-mass particles.

As a simple application, we consider the case of minimizing the shot noise in estimates of the acceleration field for an N -body model of a spherical Hernquist model. Models constructed using our scheme easily yield a factor ~ 100 reduction in the variance in the central acceleration field when compared to a traditional equal-mass model with the same number of particles. When evolving both models with a real N -body code, the diffusion coefficients in our model are reduced by a similar factor. Therefore, for certain types of problems, our scheme is a practical method for reducing the two-body relaxation effects, thereby bringing the N -body simulations closer to the collisionless ideal.

Key words: galaxies: kinematics and dynamics – methods: N -body simulations – methods: numerical.

1 INTRODUCTION

There are two types of N -body simulations in stellar dynamics. In *collisional* simulations each of the N particles represents an individual star. This type of simulation is most often used to model the evolution of star clusters in which discreteness effects, such as two-body relaxation, are important.

When it comes to modelling galaxies, however, the number of stars is large enough and the dynamical time is long enough that these discreteness effects are usually unimportant. In the limit of a very large number N of bodies, stars and dark matter particles move in a smooth mean-field potential $\Phi(\mathbf{x}; t)$ and behave as a collisionless fluid in six-dimensional phase-space (Binney & Tremaine 1987, BT87), the (mass) density at any point (\mathbf{x}, \mathbf{v}) being given by the distribution function (hereafter DF) $f(\mathbf{x}, \mathbf{v}; t)$. The time-evolution of the DF is described by the Collisionless Boltzmann Equation (hereafter CBE). Therefore, in a *collisionless* N -body simulation the N particles do not correspond to real stars; instead they provide a Monte Carlo realization of the smooth underlying DF, from which one can estimate the potential $\Phi(\mathbf{x}, t)$. By integrating the orbits of these particles, one is solving the CBE by the method of characteristics (Hernquist & Ostriker 1992, HO92; Leeuwijn Combes & Binney 1993, LCB1993)

In reality, no simulation is perfectly collisionless because

Poisson noise in the estimates of $\Phi(\mathbf{x}, t)$ inevitably leads to numerical diffusion in particles’ orbits. To reduce this noise, it is important to make N , the number of particles in the simulation, as large as possible. Unfortunately, the cost of running an N -body code scales at least linearly with N , so increasing N also makes the simulation more expensive to run. The good news is that alternative, more sophisticated weapons are available for use in the fight against small N limitations. A collisionless N -body code is essentially a Monte Carlo method and so should be amenable to well-known variance-reduction methods such as importance sampling (e.g., Press et al 1992).

In this paper we present a generally-applicable, essentially model-independent method for constructing N -body realizations of isolated model galaxies in equilibrium, suitable for use as initial conditions (hereafter ICs) in collisionless simulations. Our scheme uses importance sampling to find a sampling DF f_s that minimizes the mean-square uncertainty in a chosen set of projections of the DF f_0 . For example if modelling bar evolution, one might be most interested in following the detailed evolution of the DF around the strongest resonances. It is natural then to try to increase the sampling density near these regions by populating them with lots of low-mass particles. Outside these interesting regions, however, one must also have enough particles to maintain accurate estimations of the force field which governs the evolution of the system as a whole.

The paper is organized as follows. After reviewing the basics of Monte Carlo integration and the connection between CBE and N -body simulations, we explain our multi-mass formulation in sec-

^{*} E-mail: zhang@thphys.ox.ac.uk

[†] E-mail: magog@thphys.ox.ac.uk

tion 2.4. With the notable exception of some heuristic multi-mass schemes (e.g., Sigurdsson, Hernquist & Quinlan (1995), hereafter SHQ95, Weinberg & Katz (2007), Sellwood (2008) and Zemp et al. (2007)), most other IC-generation schemes have used equal-mass particles. In section 3 we give an example of using our scheme to suppress fluctuations in the monopole component of acceleration in a spherical galaxy model. We calculate formal estimates of the noise in N -body models constructed the equal-mass scheme (section 3.1.1) and SHQ95’s method (section 3.1.2) and compare them to our own scheme in section 3.1.3. In section 3.2 we test how well our realizations behave in practice when evolved using a real N -body code. Finally, section 4 contains a summary of the prerequisites for our scheme, along with possible scientific applications.

2 FORMULATION

2.1 Monte Carlo integration

For later reference we recall some of the basic ideas (e.g., Press et al 1992) in using Monte Carlo methods to evaluate integrals, such as

$$I = \int_D f \, dV, \quad (1)$$

of a known function f over a domain D . We first consider the case where D has unit volume: $\int_D dV = 1$. Then, given N points, $x_1 \dots x_N$, drawn uniformly from D we can estimate

$$I \simeq \frac{1}{N} \sum_{i=1}^N f(x_i) \equiv \langle f \rangle. \quad (2)$$

The variance in this estimate

$$\frac{1}{N^2} \sum_{i=1}^N [f(x_i) - \langle f \rangle]^2 \rightarrow \frac{1}{N} \left\{ \int_D f^2 \, dV - \left[\int_D f \, dV \right]^2 \right\} \quad (3)$$

as $N \rightarrow \infty$.

Now let us relax the assumption that D has unit volume and, instead of drawing points uniformly from D , let us take N points drawn from a sampling distribution f_s . We assume that f_s is normalised: $\int_D f_s \, dV = 1$. Making a straightforward change of variables and using the result above, it follows that the integral (1) can be estimated as

$$I \simeq \frac{1}{N} \sum_{i=1}^N \frac{f(x_i)}{f_s(x_i)}, \quad (4)$$

and that the variance in this estimate is approximately

$$\text{Var} I = \frac{1}{N} \left[\int_D \frac{f^2}{f_s} \, dV - I^2 \right]. \quad (5)$$

2.2 N -body simulations and the CBE

The following description of the connection between N -body simulations and the CBE borrows heavily from LCB93. We assume that the galaxy has total mass $M_* = 1$ and that the mass density of stars in phase-space is given by a DF $f(\mathbf{x}, \mathbf{v}; t) = f(\mathbf{w}; t)$, where $\mathbf{w} \equiv (\mathbf{x}, \mathbf{v})$, normalised so that

$$\int f(\mathbf{w}) \, d^6 \mathbf{w} = 1. \quad (6)$$

The evolution of the DF is governed by the CBE,

$$\frac{\partial f}{\partial t} + \mathbf{v} \cdot \frac{\partial f}{\partial \mathbf{x}} - \frac{\partial \Phi}{\partial \mathbf{x}} \cdot \frac{\partial f}{\partial \mathbf{v}} = 0. \quad (7)$$

It conserves phase-space density, so that

$$f(\mathbf{w}(t); t) = f(\mathbf{w}_0; 0), \quad (8)$$

where $\mathbf{w}(t)$ is the path traced by an individual particle, with $\mathbf{w}_0 \equiv \mathbf{w}(t = 0)$. As HO92 and LCB93 point out, in a collisionless N -body simulation one is solving the CBE for these $\mathbf{w}(t)$ by integrating the characteristic equation,

$$\frac{d\mathbf{w}}{dt} = \frac{d\mathbf{x}}{dt} = \frac{d\mathbf{v}}{dt} = \mathbf{a}, \quad (9)$$

and using Monte Carlo integration to estimate the acceleration

$$\mathbf{a}(\mathbf{x}; t) \equiv -\frac{\partial \Phi}{\partial \mathbf{x}} = -G \nabla \int \frac{f(\mathbf{w}'; t)}{|\mathbf{x} - \mathbf{x}'|} \, d^6 \mathbf{w}'. \quad (10)$$

From (4) it follows that

$$\mathbf{a}(\mathbf{x}; t) \simeq -G \nabla \sum_{i=1}^N \frac{m_i}{|\mathbf{x} - \mathbf{x}_i|}, \quad (11)$$

corresponding to a distribution of N point particles with masses

$$m_i = \frac{1}{N} \frac{f(\mathbf{w}_i; t)}{f_s(\mathbf{w}_i; t)}. \quad (12)$$

These m_i clearly depend on the choice of sampling DF f_s . The simplest choice is $f_s(\mathbf{w}; t) = f(\mathbf{w}; t) = f(\mathbf{w}_0; 0)$, in which case all particles have equal masses $m_i = 1/N$. However, one is free to tailor the choice of f_s to suit the particular problem under study.

The singularities in (11) at $\mathbf{x} = \mathbf{x}_i$ yield estimates of $\mathbf{a}(\mathbf{x})$ that suffer from unacceptably large scatter; in fact, they correspond to the direct accelerations appropriate for a collisional N -body code! So, in practice collisionless simulations do not use (11) directly, but instead obtain $\mathbf{a}(\mathbf{x})$ using techniques (e.g., softened force kernels, grid methods or truncated basis-function expansions) that reduce the scatter by removing the singularities. More generally, eq. (11) provides only the most simple-minded estimate of the integral (10), and one has some leeway in how one reconstructs $f(\mathbf{w}; t)$ from the discrete realization furnished by the N particles. Of course, the reliability of any sensible reconstruction will be wholly dependent on how well the DF is sampled.

2.3 Observables

What constitutes a “good” choice of sampling density f_s ? The DF f is a high-dimensional probability density and itself is not measurable. We are usually only interested in coarse-grained projections of the DF,

$$\langle Q_i \rangle \equiv \int f(\mathbf{w}) Q_i(\mathbf{w}) \, d^6 \mathbf{w}, \quad (13)$$

where the kernels $Q_i(\mathbf{w})$ are some functions of the phase-space coordinates (\mathbf{x}, \mathbf{v}) . For the purposes of the present paper, we consider a “good” sampling scheme to be one that minimizes the uncertainty in the estimates of some given set of $\langle Q_i \rangle$. Apart from some general guidance, we do not address the question of how best to choose these Q_i , which usually requires some experience of the particular problem at hand.

We now give some examples. It is helpful to introduce the indicator function

$$\mathbb{1}_V(\mathbf{w}) \equiv \begin{cases} 1, & \text{if } \mathbf{w} \in V \\ 0, & \text{otherwise.} \end{cases} \quad (14)$$

Then a particularly simple but important choice of kernel is

$$Q_i(\mathbf{w}) = \mathbb{1}_{V_i}(\mathbf{w}), \quad (15)$$

for which $\langle Q_i \rangle$ measures the mass inside a volume V_i . For many problems one might choose some of the V_i to surround important resonances in phase-space, so that $\langle Q_i \rangle$ measures the phase-space density around the resonances. With appropriate choices of projection kernel Q_i , the expression (13) includes quantities such as the galaxy's density profile, its velocity moments or even its projected line-of-sight velocity distributions.

More fundamentally, an N -body model should provide a good estimate of the galaxy's acceleration field. Therefore we recommend that many of the $\langle Q_i \rangle$ be used to measure at least the monopole component of the galaxy's acceleration field at a range of points. This can be achieved using (15) with spherical volumes V_i centred on $\mathbf{x} = 0$ for a range of radii r_i , encompassing all velocity space for $|\mathbf{x}| < r_i$. Similarly, one can include higher-order multipole components of the galaxy's acceleration field by choosing a slightly more complicated projection kernel Q_i (see equation 35 below).

2.4 Optimal sampling scheme

The problem we address in this paper is the following. We wish to construct an equilibrium N -body realization of a galaxy model with some known DF f_0 . Specifically, we seek ICs that faithfully represent some projections,

$$\langle Q_i \rangle = \int f_0 Q_i d^6 \mathbf{w}, \quad (16)$$

of this DF, for a set of n_Q kernels $Q_i(\mathbf{w})$. What is the “best” choice of sampling DF f_s given this f_0 and choice of kernels Q_i ?

More formally, from (5) the uncertainty in a Monte Carlo estimate of $\langle Q_i \rangle$ obtained using N particles drawn from the sampling distribution f_s is given by

$$\text{Var} \langle Q_i \rangle = \frac{1}{N} \left[\int \frac{f_0^2}{f_s} Q_i^2 d^6 \mathbf{w} - \langle Q_i \rangle^2 \right]. \quad (17)$$

Notice that, unlike most introductory textbook examples of Monte Carlo methods, we have n_Q such estimates but just one f_s . We seek a normalised sampling DF f_s that minimizes the mean-square fractional uncertainty

$$S \equiv \sum_{i=1}^{n_Q} (\delta Q_i)^2 \quad (18)$$

where δQ_i , the formal relative uncertainty in a measurement of Q_i , is given by

$$(\delta Q_i)^2 \equiv \frac{\text{Var} \langle Q_i \rangle}{\langle Q_i \rangle^2}. \quad (19)$$

Of course there are many other possible measures of the “goodness” of some choice of f_s .

One can immediately use the Euler–Lagrange equation to show that choosing

$$f_s^2(\mathbf{w}) \propto f_0^2(\mathbf{w}) \sum_{i=1}^{n_Q} \frac{Q_i^2(\mathbf{w})}{\langle Q_i \rangle^2} \quad (20)$$

extremizes (18), the proportionality constant being set by the constraint that f_s should be normalized, $\int f_s d^6 \mathbf{w} = 1$. This direct solution is flawed, however, since for most interesting choices of Q_i the resulting f_s depends on orbit phase; using this f_s the masses of particles sampling a given orbit would vary along the orbit! Therefore in practice we use a slightly less direct approach.

We partition phase space into n_f cells and write τ_j^{-1} for the phase-space volume enclosed by the j^{th} cell. We parametrize f_s as

$$f_s(\mathbf{w}) = \sum_{j=1}^{n_f} \frac{\mathbb{1}_{\tau_j}}{a_j} f_0(\mathbf{w}), \quad (21)$$

so that within the j^{th} phase-space cell f_s is given by $f_0(\mathbf{w})/a_j$. For the equilibrium models considered, it is natural to choose τ_j to be cells in integral space. Substituting this f_s into (19) yields

$$(\delta Q_i)^2 = \frac{1}{N} \left[\sum_{j=1}^{n_f} a_j H_{ij} - 1 \right], \quad (22)$$

where

$$H_{ij} \equiv \frac{\int_{\tau_j} f_0 Q_i^2 d^6 \mathbf{w}}{\langle Q_i \rangle^2}. \quad (23)$$

If we further define

$$H_j \equiv \sum_{i=1}^{n_Q} H_{ij}, \quad (24)$$

then the mean-square fractional uncertainty (18) becomes

$$S = \frac{1}{N} \left[\sum_{j=1}^{n_f} a_j H_j - n_Q \right]. \quad (25)$$

Our goal is to find the coefficients a_j that minimize this S , subject to the constraint that the resulting f_s be normalised. The normalisation constraint is that

$$\int f_s d^6 \mathbf{w} = \sum_{j=1}^{n_f} \frac{I_j}{a_j} = 1, \quad (26)$$

where

$$I_j \equiv \int_{\tau_j} f_0 d^6 \mathbf{w}. \quad (27)$$

Using the method of Lagrange multipliers, the coefficients of the “best” sampling DF obtained by minimizing (25) subject to the constraint (26) are simply

$$a_j = \sqrt{\frac{I_j}{H_j}} \sum_{k=1}^{n_f} \sqrt{I_k H_k}, \quad (28)$$

which is just the direct solution (20) in disguise, but averaged over the phase-space cells τ_j and correctly normalized. This averaging means that the resulting f_s will be smooth, provided that none of the kernels Q_i pick out specific regions of integral space.

Substituting the f_s given by (21) into (12), we have that particles in phase-space cell τ_j have masses $m_j = a_j/N$. One can therefore easily impose additional, direct constraints on the masses of particles within a subset of the phase-space cells τ_j ; simply repeat the minimisation of (25) subject to (26) while holding the relevant subset of the a_j fixed at the desired values. For example, when generating an N -body realization of a dark-matter halo model inside which one intends to embed a disk of light particles, one might want to ensure that those halo particles passing through the disk have the same mass as the disk particles. Of course, a more pedestrian approach would be to introduce additional kernels Q_i to pick

¹ Note that we use V to denote subvolumes of phase-space be used in the calculation of the projections (13) of the DF f_0 , and τ for the subvolumes used in the discretization of the sampling DF f_s .

out the relevant parts of integral space. We caution, however, that we have not tested how well such a “bumpy” f_s would work in practice; the tests we present later all involve smoothly varying sampling distributions.

2.5 ICs for N -body model

Together with f_0 , the coefficients a_j completely determine the sampling DF f_s of the form (21). In particular, it reduces to the conventional equal-mass case when all $a_j = 1$.

We apply the following sequence of steps N times to draw particles from this f_s , thereby constructing an N -body realization of the galaxy model:

(1) Choose one of the n_f cells at random, the probability of choosing the j^{th} cell being given by I_j/a_j . Let i be the index of the chosen cell.

(2) Assign a mass $m_i \equiv f_0(\mathbf{w}_i)/Nf_s(\mathbf{w}_i) = a_i/N$ to the particle.

(3) Within the i^{th} cell, draw \mathbf{x}_i from its density distribution, $\rho_i = \int f_0 \mathbb{1}_{\tau_i} d^6\mathbf{w}$. For the special case of a spherical galaxy, one can precompute the cumulative mass distribution $M_i(r)$ for each of the n_f cells and use this to draw a radius r_i , followed by angles θ_i and ϕ_i .

(4) Use an acceptance-rejection method to draw \mathbf{v}_i from $f_0(\mathbf{x}_i, \mathbf{v})$ at this fixed value of \mathbf{x}_i .

3 AN EXAMPLE

In this section we use a simple galaxy model to demonstrate our scheme. Our galaxy model is spherical and isotropic, with density profile (Hernquist 1990)

$$\rho(r) = \frac{M_*}{2\pi r(r+a)^3}, \quad (29)$$

total mass M_* and scale radius a . By Jean’s theorem, the model’s DF $f(\mathbf{x}, \mathbf{v})$ depends on (\mathbf{x}, \mathbf{v}) only through the binding energy per unit mass \mathcal{E} . Hernquist (1990) gives an expression for $f(\mathcal{E})$.

We want to construct an N -body realization of this model that minimizes the mean-square error in the monopole component of the acceleration averaged over many decades in radius, from $r_{\min} = 10^{-4}a$ up to $r_{\max} = 10^2a$. To achieve this we choose kernels $Q_i = \mathbb{1}_{V_i}(r)$ that measure the mass enclosed within a sequence of 25 spheres centred on the origin, with radii r_i spaced logarithmically between r_{\min} and r_{\max} . We use (22) to calculate the formal uncertainty δM_i in the enclosed mass for a range of discretized sampling densities of the form (21), including (28).

To implement this, we first of all partition integral space (\mathcal{E}, J^2) onto a regular $n_f = n_{\mathcal{E}} \times n_X$ grid. The $n_{\mathcal{E}}$ energies \mathcal{E}_j are chosen to match the potential $\mathcal{E}_j = \Psi(r_j)$ with r_j logarithmically spaced between $10^{-6}a$ and 10^3a . At each \mathcal{E}_j , there are n_X values of X_{jk} running linearly from 0 to 1, where $X_{jk} = J_k(\mathcal{E}_j)/J_c(\mathcal{E}_j)$ is the orbital angular momentum normalised by the circular angular momentum at energy \mathcal{E}_j ². These choices ensure that our f_s samples well the interesting parts of phase-space. For the calculations below we take $n_{\mathcal{E}} \times n_X = 200 \times 100$, although a coarser grid (e.g., 50×25) would suffice. Having defined our projection kernels $Q_i = \mathbb{1}_{V_i}$, we use (16) to calculate the expected values of

² $X = J(\mathcal{E})/J_c(\mathcal{E})$ is a measure of an orbit’s circularity; orbits with $X = 1$ are perfectly circular, while those with $X = 0$ are perfectly radial.

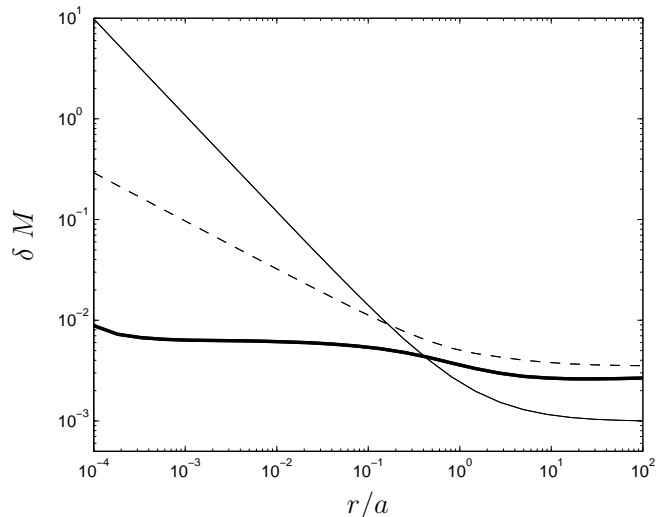


Figure 1. Formal relative errors $\delta M \equiv (\text{Var} \langle M \rangle)^{1/2} / \langle M \rangle$ (eq. 19) in the monopole component of the potential of a Hernquist model (eq. 29) constructed using the same number $N = 10^6$ of particles, but drawn from different sampling DFs. The heavy solid curve plots results for our tailored sampling DF. For comparison, we also show results for the conventional equal-mass scheme (light solid curve) and Sigurdsson et al.’s (1995) heuristic multi-mass scheme (dashed curve).

enclosed mass $\langle M_i \rangle$ and the ancillary quantities H_{ij} (from eq. 23), and use these to obtain the formal uncertainties δM_i in (22).

3.1 Comparison with other schemes: formal errors

Before applying our method, we study two other schemes: the conventional equal-mass scheme and the multi-mass scheme of Sigurdsson, Hernquist & Quinlan (1995).

3.1.1 The conventional equal-mass scheme

The most common (albeit implicit) choice of sampling density is $f_s = f_0$, which corresponds to setting all $a_j = 1$ in our equation (21). All particles then have the same $1/N$ mass. For our example Hernquist model the fraction of particles within radius r is $r^2/(a+r)^2$, so that less than 1% of the particles are within $0.1a$. As shown in figure 1, for this f_s the formal uncertainty $\delta M(r)$ rises steeply towards the centre. Although this scheme produces accurate estimates of the galaxy’s potential outside the scale radius a , it performs poorly in the interesting r^{-1} central density cusp.

3.1.2 Sigurdsson et al.’s multi-mass scheme

Sigurdsson, Hernquist & Quinlan (1995) have used an interesting heuristic scheme to improve the resolution of N -body models near galaxy centres. In effect, they use an anisotropic sampling function of the form (21) with coefficients

$$a(\tau) \equiv B \times \begin{cases} \left(\frac{r_{\text{peri}}(\tau)}{a}\right)^\lambda & \text{if } r_{\text{peri}} < a, \\ 1 & \text{otherwise,} \end{cases} \quad (30)$$

where $r_{\text{peri}}(\tau)$ is the smallest pericentre radius of any orbit from the phase-space cell τ , and the constant B is chosen to normalize f_s . When the parameter $\lambda = 0$, then $a_j = 1$ and the sampling

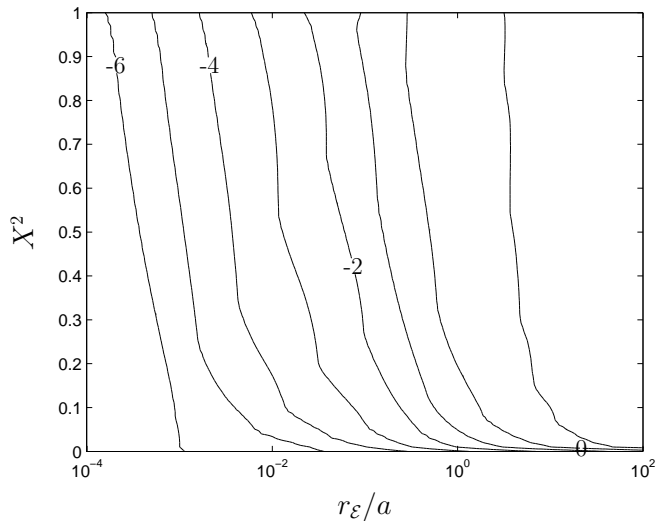


Figure 2. Contour map of $\log_{10}(f_s/f_0)$ for the optimal multi-mass sampling scheme of section 3.1.3; notice the strong enhancement in low angular momentum and large energy (small r_E) region. These correspond to orbits with small peri-centre radii.

DF f_s is identical to f_0 . Increasing λ improves the sampling of the cusp by increasing the number density of particles having peri-centres $r_{\text{peri}} < a$. Consequently, as $r \rightarrow 0$ the number density of particles rises more rapidly than the mass density, permitting better resolution in the centre. To balance this increase in number density, each particle is assigned a mass $f_0/Nf_s = a_j/N$ so that the phase-space mass density is still given by the desired f_0 .

The dashed curve in figure 1 shows the formal error $\delta M(r)$ in our implementation of their scheme for $\lambda = 1$. Their scheme does much better than the conventional equal-mass scheme at small radii $r \ll a$, at the cost of a slightly noisier monopole at $r \gtrsim a$.

3.1.3 Our scheme

It is encouraging to see that SHQ95’s multi-mass scheme does, to some extent, improve mass resolution at small radius. However, as shown in figure 1, δM at $r = 10^{-4}a$ is still almost two orders of magnitude larger than at $r = a$. Can we achieve even better results by carefully designing an f_s that generates a flat $\delta M(r)$ across a large range of radii?

The f_s given by our optimal choice of coefficients (28) is plotted in figure 2. It is qualitatively similar to SHQ95’s results, in the fact that it samples densely the low-angular momentum parts of phase-space. The detailed shape of the function is different, however, and the thick solid curve in figure 1 shows that our scheme provides much better estimates of the monopole components of the acceleration at small radii; in fact, the formal error $\delta M(r)$ varies by only a factor ~ 4 over six decades in radius.

3.2 N -body realizations

Figure 3 shows the spectrum of masses obtained using the algorithm detailed in §2.5 to draw $N = 10^6$ particles from this optimal f_s . Unlike the conventional scheme which would give all particles the same $10^4 M_\odot$ mass if assuming $M_* = 10^{10} M_\odot$, our multi-mass scheme assigns a range of masses between $10^{-2} M_\odot$ and

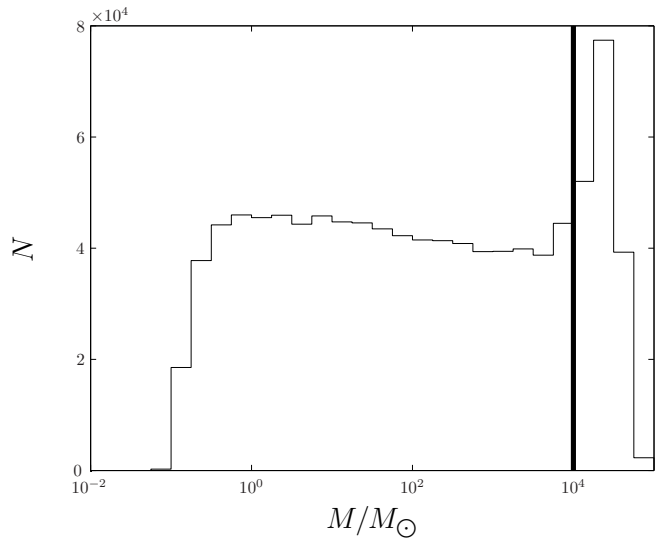


Figure 3. Histogram of particle masses from an $N = 10^6$ multi-mass realization of a Hernquist galaxy, scaled to a total mass $M_* = 10^{10} M_\odot$. The span of 8 decades in mass gives sub-solar mass resolution in “interesting” regions of phase space. In contrast, in an equal-mass realization all particles would have mass $10^4 M_\odot$ (thick solid line).

$10^6 M_\odot$ (8 decades), with many low-mass particles in the central region.

As a simple sanity check of our formal estimates of the errors in the monopole, we count the mass of particles within the same spheres V_i used to calculate δM_i . The deviations from the mass profile of the target Hernquist model are consistent (figure 4) with the expected values of δM from equation (22).

Ultimately, the purpose of our sampling scheme is to improve the numerical modelling of collisionless galaxies close to equilibrium using full N -body integrations. To test how well our scheme succeeds at this task, we use the particle-multiple-mesh code Grommet (Magorrian 2007) to compare the evolution of our multi-mass models against equal-mass ones. Below, we adopt N -body units $G = M = a = 1$.

3.2.1 How well is the acceleration field reproduced?

An important unsolved problem is how best to estimate the accelerations (10) given a discrete N -particle realization of the underlying DF f . The most sophisticated approaches to this problem (e.g., Dehnen (2001) and references therein) have focused on finding softening kernels that minimize the errors in the acceleration field given a static distribution of N equal-mass particles. In the present paper we do not investigate how different softening lengths or softening kernels affect our multi-mass models. We simply adopt a nested series of boxes with boundaries at $|x| = 100 \times 2^{-i}$ with $i = 0, \dots, 20$, each box covered by a 60^3 mesh. As one moves to smaller length scales the effective softening length decreases, with $\epsilon_{\text{min}} = 200/60 \times 2^{-20} \approx 10^{-4}$.

Figure 4 shows the fractional error in the radial component of the acceleration field returned by Grommet, in addition to the fractional error in enclosed mass. There is an approximately constant offset between these two quantities for equal- and multi-mass realization. Since our ICs here have been tailored to minimize the variance in the monopole component of the acceleration field, how important is our neglect of the higher-order multipoles?

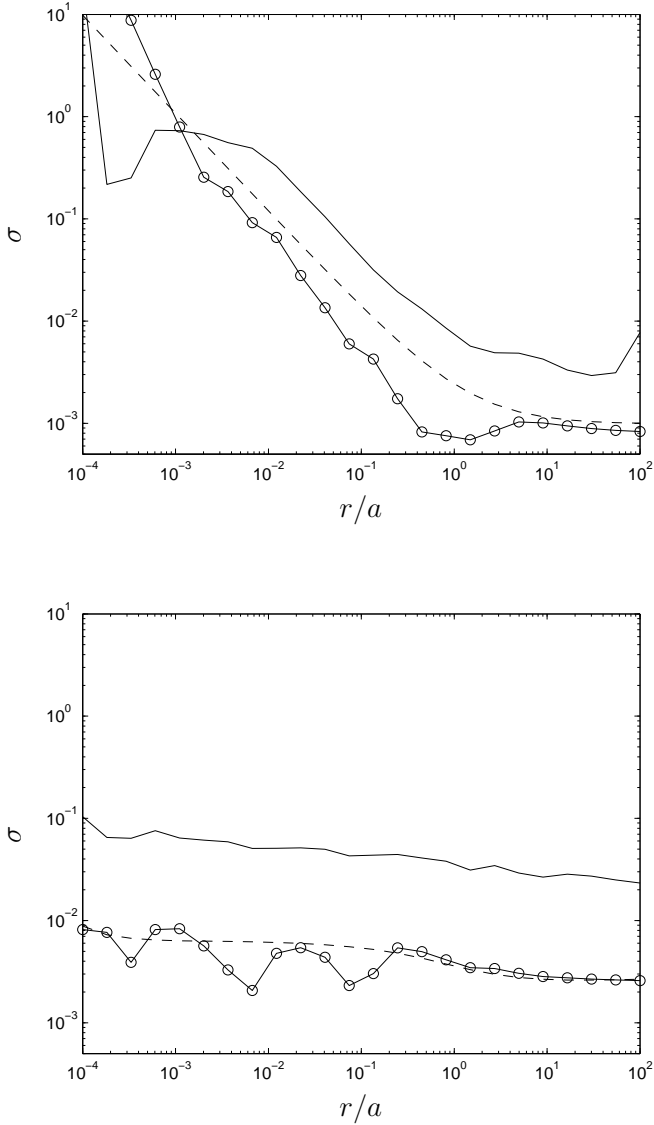


Figure 4. RMS fractional deviations in acceleration (solid line), in mass (circle-solid line) together with its analytical value δM in dashed line; top panel for equal-mass model and bottom panel for multi-mass model. For this single acceleration calculation, we include 16 levels of refinements and therefore all the values should be believable outside $\epsilon_{\min} \approx 10^{-4}$.

In terms of multipole moments, the radial component of the acceleration is (e.g., BT87)

$$a_r(r, \theta, \phi) = 4\pi G \sum_{lm} \frac{Y_l^m}{2l+1} \times \left[-\frac{l+1}{r^{l+2}} \int_0^r \rho_{lm}(r') r'^{l+2} dr' + l r^{l-1} \int_r^\infty \rho_{lm}(r') \frac{dr'}{r'^{l-1}} \right] \quad (31)$$

where

$$\rho_{lm}(r) = \int_0^{2\pi} d\phi \int_0^\pi d\theta \sin \theta Y_l^{m*}(\theta, \phi) \rho(r, \theta, \phi). \quad (32)$$

This can be rewritten as

$$a_r(r, \theta, \phi) = -\frac{4\pi G}{r^2} \sum_{lm} \langle M_{lm}(r) \rangle Y_l^m(\theta, \phi), \quad (33)$$

where $\langle M_{lm}(r) \rangle$ are given by

$$\langle M_{lm}(r) \rangle = \int f_0(\mathbf{w}') M_{lm}(r, \mathbf{w}') d^6 \mathbf{w}' \quad (34)$$

with projection kernels

$$M_{lm}(r, \mathbf{w}') = Y_l^{m*}(\theta', \phi') \left[\frac{l+1}{2l+1} \frac{r'^l}{r^l} \mathbb{1}_{V(r)}(\mathbf{w}') - \frac{l}{2l+1} \frac{r'^{l+1}}{r^{l+1}} \mathbb{1}_{\overline{V(r)}}(\mathbf{w}') \right], \quad (35)$$

where $V(r)$ encompasses all phase-space points having radii less than the (real-space) radius r , and $\overline{V(r)}$ is its complement. For our spherical galaxy,

$$\langle M_{lm}(r) \rangle = \int f_0(\mathbf{w}') M_{lm}(r, \mathbf{w}') d^6 \mathbf{w}' = \begin{cases} M(r), & \text{if } l = m = 0 \\ 0, & \text{otherwise.} \end{cases} \quad (36)$$

The corresponding variance in $a_r(r)$ for an N -body realization drawn from some choice of f_s is

$$\text{Var} \langle a_r(r) \rangle = \frac{4\pi G}{r^2} \sum_{lm} \text{Var} \langle M_{lm}(r) \rangle Y_l^m(\theta, \phi), \quad (37)$$

where, from (17),

$$\text{Var} \langle M_{lm}(r) \rangle = \frac{1}{N} \left[\int \frac{f_0^2(\mathbf{w}')}{f_s(\mathbf{w}')} M_{lm}(r, \mathbf{w}')^2 d^6 \mathbf{w}' - \langle M_{lm}(r) \rangle^2 \right]. \quad (38)$$

Similarly, the variance in the tangential component of acceleration field can be achieved by using projection kernels

$$\text{Var} \langle a_{\theta, \phi}(r) \rangle = \frac{4\pi G}{r^2} \sum_{lm} \text{Var} \langle M_{lm}^t(r) \rangle [Y_l^m(\theta, \phi)]'_{\theta, \phi}, \quad (40)$$

where

$$M_{lm}^t(r, \mathbf{w}') = Y_l^{m*}(\theta', \phi') \left[\frac{1}{2l+1} \frac{r'^l}{r^l} \mathbb{1}_{V(r)}(\mathbf{w}') + \frac{1}{2l+1} \frac{r'^{l+1}}{r^{l+1}} \mathbb{1}_{\overline{V(r)}}(\mathbf{w}') \right]. \quad (41)$$

So, given any choice of f_s , we can use the expressions above to calculate the contribution of the higher-order multipole moments to the formal errors in the acceleration. We find that, as we progressively include more terms, our estimate of the formal $\text{Var} \langle a_r(r) \rangle$ approaches the actual errors observed in the N -body realization.

Alternatively, we can find our optimal sampling DF f_s by minimizing

$$S \equiv \frac{\sum_{i=1}^{n_Q} \sum_{l=0}^{l_{\max}} \sum_{m=-l}^l \text{Var} \langle M_{lm}^i \rangle}{\langle M_i \rangle^2}, \quad (42)$$

truncated at say $l_{\max} = 2$. Notice that this new S reduces to the old one in eq. (18) when $l_{\max} = 0$, but otherwise includes additional terms with $l > 0$, each weighted by the monopole component $l = 0$. On increasing l_{\max} from 0 to 2, the formal $\text{Var} \langle a_r(r) \rangle$ increases but the shape of the curve remains approximately unchanged and there are no noticeable differences in the resulting f_s . Therefore, our neglect of higher-order multipole moments is justified, at least in the present case, provided one bears in mind that the errors in the full acceleration field are going to be larger by an approximately constant factor than what one would estimate from the monopole component alone.

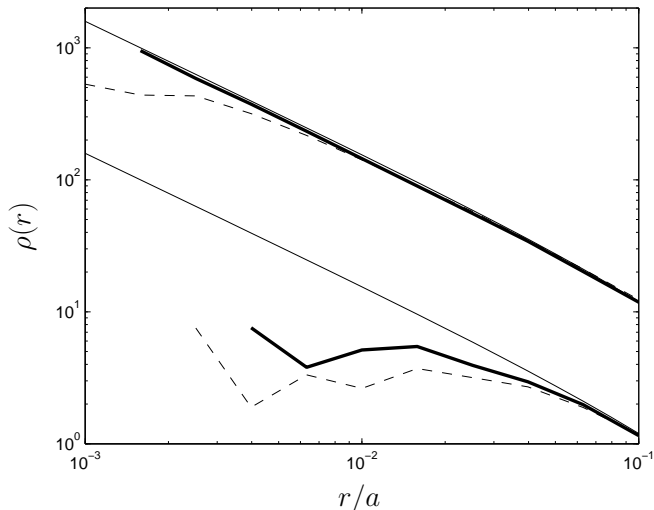


Figure 5. Inner density profile of a multi-mass (top set of curves) and an equal-mass (lower, offset by 10 vertically) realizations of the same Hernquist model evolved for 200 time units using the Grommet N -body code. The ICs in each case are plotted as the heavy solid curves. The dashed curves show profiles after the model has been evolved for 200 time units.

3.2.2 How well are integrals of motion conserved?

This paragraph describes the details of a full N -body implementation. Using both equal and multi-mass schemes, we draw 10^6 particles with radii between $10^{-3} < r < 10^2$. In order to suppress slightly deviance from symmetry (the odd terms of higher-order multipoles) and remove any intrinsic transient in linear momentum (see also McMillan & Dehnen 2005), ICs (\mathbf{x}, \mathbf{v}) are extended to include the mirror distribution by reflecting each of the 10^6 particles with $(\mathbf{x}, \mathbf{v}) \rightarrow (-\mathbf{x}, -\mathbf{v})$. The full ICs then have $N = 2 \times 10^6$ particles. Taking the efficiency of integration into consideration, only a 12-level nested series of boxes each covered by a 60^3 mesh is used, together with a single time-step of 2×10^{-4} . Therefore, we expect our numerical results to be trustworthy at radii greater than a few times 10^{-3} .

Figure 5 plots the inner density profiles of both realizations after evolving each for 200 time-units (or 300 circular orbit periods at $r = 0.01$). The lack of particles at small radius $r \sim 10^{-2}$ in the equal-mass realization means that the initial model is out of exactly-detailed equilibrium and causes the central density profiles to flatten. In contrast, the density profile in the multi-mass case is always much better behaved there.

It is interesting to examine what is going on at the level of individual orbits. Both realizations begin with spherical symmetry and remain spherical, apart from the effects of Poisson noise. The amount of diffusion in the angular momentum J of each particle's orbit serves as a strong gauge of relaxation effects. This is complicated by the fact that many particles in isotropic models being considered here have $J(t = 0) \simeq 0$. In such cases, even a small change in $J(t > 0)$ would yield a large fractional change when measured in respect to its initial value. To circumvent this artificial problem, for each particle we measure the change in angular momenta relative to its circular value at $t = 0$ using

$$\Delta X_i^2 = \left[\frac{J_i(t) - J_i(0)}{J_c(\mathcal{E}_i)} \right]^2 \frac{1}{t}. \quad (43)$$

Binning particles by energy and calculating the mean ΔX_i^2 within

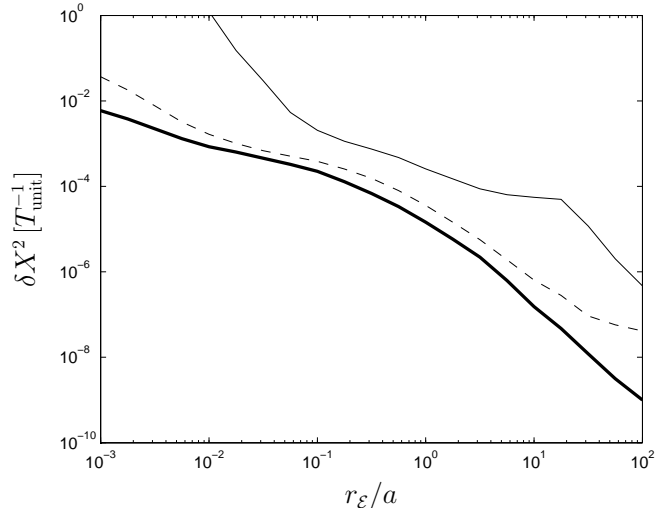


Figure 6. Time-average diffusion rate δX^2 (eq. 43) against energy labelled radius $r_{\mathcal{E}}$ measured between $t = 0$ and $t = 200$ for a multi-mass realization evolved using Grommet (thick curve), falCON (dashed) and for an equal-mass realization evolved using Grommet (thin curve).

each energy bin gives us the time-averaged diffusion rate $\delta X^2(\mathcal{E})$. As shown in figure 6, both models suffer diffusion, but due to the enhancement of particle numbers and hence the smoothness of potential field in the central region, diffusion in the multi-mass scheme is suppressed by two orders of magnitude across the whole system.

As a further test of the robustness of our multi-mass scheme, we have evolved our multi-mass ICs using the tree code FALCON Dehnen (2000) with a single interparticle softening radius of 10^{-3} , comparable to the finest mesh size used in the Grommet runs. The dashed curve in figure 6 plots the resulting δX^2 ; our scheme works just as well for tree codes as it does for mesh codes, although the variable softening in Grommet does slightly decrease the amount of diffusion. This is not surprising, since the only difference between the two runs is the approximations used to estimate the accelerations (10).

In any model with a broad spectrum of particle masses, a natural question is what happens if heavy bodies from the outskirts visit the centre full of light mass elements and vice versa. To address this issue, we have measured the $\delta X^2(\mathcal{E})$ of equation (43) but, instead of considering all particles of a given \mathcal{E} , we compare the diffusion of particles on radially-biased orbits with $X^2 < 0.1$ to those on nearly-circular orbits with $X^2 > 0.9$. As shown in figure 7, there are no systematic differences between them. The reason for this is simply that particles with $X \simeq 0$ spend most of their time at apocentre, the apocentre radius being only a factor ~ 2 larger than the radius of a circular orbit of the same energy. Nevertheless, a particle with $X \simeq 0$ will affect all of the more tightly bound orbits as it plunges through the centre of the galaxy, but our measured diffusion rates account for this.

4 CONCLUSIONS

We have presented a general multi-mass scheme to construct Monte Carlo realizations of collisionless galaxy models with known steady-state DFs f_0 . The scheme uses importance sampling to find the tailored sampling DF f_s that minimizes the sum of mean-square uncertainties in a given set of observable quantities of the form (16).

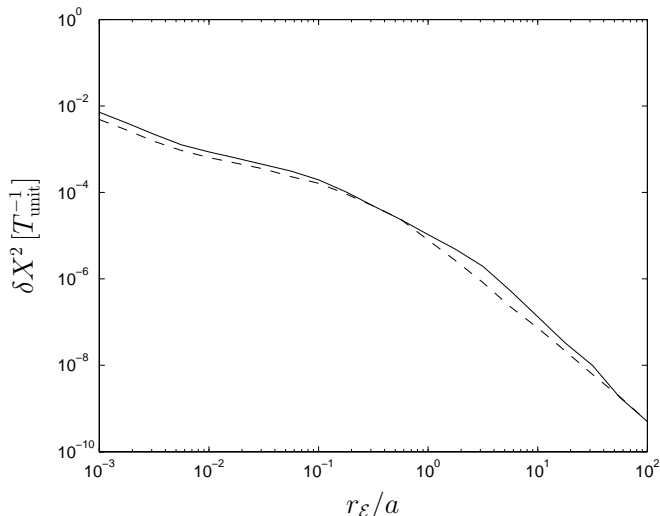


Figure 7. δX^2 in multi-mass simulations for particles with $X^2 < 0.1$ (dashed curve) and $X^2 > 0.9$ (solid).

Although our method works for any reasonably general collisionless N -body code, we note that there are three conditions that must be satisfied before it can be applied successfully:

(i) The system should be in a steady state, or close to one.

(ii) The DF f_0 should be quick and cheap to evaluate, either numerically or analytically. The calculation of f_s is not much more demanding for axisymmetric or triaxial galaxies than for spherical isotropic models. Finding f_0 for such systems is, however, non-trivial since one rarely has sufficient knowledge of the underlying potential's integrals of motion, but suitable flattened DFs do exist, including the standard axisymmetric two-integral $f(\mathcal{E}, L_z)$ models and also rotating triaxial models such as those used in, e.g., Berczik et al. (2006). An alternative way of constructing flattened multi-mass realizations would be to apply Holley-Bockelmann et al. (2002)'s adiabatic sculpting scheme to a spherical N -body model constructed using our scheme.

(iii) Finally, the utility of our multi-mass scheme depends critically on the selection of the projection kernels $Q_i(\mathbf{w})$.

Point (ii) is a well-known and longstanding problem, but the final condition is new. It is probably best addressed by experimenting with different sets of kernels, especially since it is easy to test the consequences of modifying them. Nevertheless, there are cases in which modest physical insight offers some guidance on choosing the Q_i . Here are some examples.

Galaxies with central massive black holes It is straightforward to extend our treatment of self-consistent galaxy models to models containing a central black hole (hereafter MBH). By choosing kernels (as in section 3) to measure *the monopole component of galaxy's force field* and choosing f_s to minimize their mean-square fractional uncertainty, one also achieves better spatial and mass resolution within the sphere of influence of the black hole.

Loss-cone problems The rate of supplying stars into MBH's loss-cone is an important ingredient in galaxy models with central MBHs. A thorough understanding of collisionless loss-cone refilling mechanisms and accurate estimates of the resulting refilling rates are particularly critical for the prediction of astrophysical quantities such as the timescale of binary MBH merger (Begelman et al. 1980; Yu 2002; Milosavljević & Merritt 2003), the tidal disruption rate of stars (Syer & Ulmer 1999; Magorrian & Tremaine

1999; Wang & Merritt 2004). When using N -body simulations to study such loss-cone problems, one is often interested in *stars on low angular momentum orbits* and can therefore choose kernels to pick out such loss-cone phase-space for detailed modelling, while simultaneously maintaining accurate estimates of the galaxy's acceleration field.

Sinking satellites Kazantzidis et al. (2004) demonstrate the significance of using equilibrium N -body realizations of satellite models when investigating the effect of tidal stripping of CDM substructure halos (satellites) orbiting inside a more massive host potential. Besides the shape of the background potential and the amount of tidal heating, the mass-loss history is very sensitive to the detailed density profile of the satellite itself. One can therefore make one step further from equal-mass realizations by designing kernels to pick out *orbits that pass through the tidal radius*, while again maintaining an accurate estimate of the satellite's acceleration field.

ACKNOWLEDGEMENTS

We thank James Binney for helpful discussions and an anonymous referee for comments that helped improve the clarity of this paper. MZ's work is supported by Dorothy Hodgkin Postgraduate PPARC-BP Awards. JM thanks the Royal Society for financial support.

REFERENCES

- Begelman, M. C., Blandford, R. D., & Rees, M. J. 1980, *Nature*, 287, 307
- Berczik, P., Merritt, D., Spurzem, R., & Bischof, H.-P. 2006, *ApJL*, 642, L21
- Binney J., Tremaine S., 1987, *Galactic Dynamics*. Princeton Univ. Press, Princeton, NJ (**BT87**)
- Dehnen, W. 2000, *ApJL*, 536, L39
- Dehnen W., 2001, *MNRAS*, 324, 273
- Hernquist L., 1990, *ApJ*, 356, 359
- Hernquist L. & Ostriker J.R., 1992, *ApJ*, 386, 375H (**HO92**)
- Holley-Bockelmann, K., Mihos, J. C., Sigurdsson, S., Hernquist, L., & Norman, C., 2002, *ApJ*, 567, 817
- Kazantzidis, S., Magorrian, J., & Moore, B. 2004, *ApJ*, 601, 37
- Leeuwijn F., Combes F. & Binney J., 1993 *MNRAS*, 262, 1013 (**LCB93**)
- Magorrian, J., & Tremaine, S. 1999, *MNRAS*, 309, 447
- Magorrian, J. *MNRAS*, 381, 1663 (**M07**)
- McMillan P. J., Dehnen W., 2005, *MNRAS*, 363, 1205
- Milosavljević, M., & Merritt, D. 2003, *ApJ*, 596, 860
- Press W.H., Flannery B.P., Teukolsky S.A., Vetterling W.T., 1992, *Numerical Recipes in C*, 2nd edn. Cambridge Univ. Press, Cambridge
- Sellwood J., astro-ph/0610468
- Sigurdsson S., Hernquist L., & Quinlan G. D. 1995, *ApJ*, 446, 75 (**SHQ95**)
- Syer, D., & Ulmer, A. 1999, *MNRAS*, 306, 35
- Tremaine, S., Richstone, D. O., Byun, Y.-I., Dressler, A., Faber, S. M., Grillmair, C., Kormendy, J., & Lauer, T. R. 1994, *AJ*, 107, 634
- Wang, J., & Merritt, D. 2004, *ApJ*, 600, 149
- Weinberg M. D., Katz N., 2007, *MNRAS*, 375, 460
- Yu, Q. 2002, *MNRAS*, 331, 935

Zemp, M., Moore, B., Stadel, J., Carollo, C. M., & Madau, P.
2007, ArXiv e-prints, 710, arXiv:0710.3189

This paper has been typeset from a $\text{\TeX}/\text{\LaTeX}$ file prepared by the author.